



In-situ

K. C. Wang, L. H. Cheng, C. L. Wang, K. S. Ess, L. L. Gao, T. P. Jia

Gemological Institute, China University of Geosciences, Wuhan 430074, PR China
 Hubei Gem and Jewelry Engineering Technology Research Center, Wuhan 430074, PR China
 School of Materials Science and Engineering, Huazhong University of Science and Technology, Wuhan 430074, PR China
 Mechanical Engineering, University of Birmingham, Birmingham B15 2TT, UK
 School of Electrical and Electronic Engineering, Huazhong University of Science and Technology, Wuhan 430074, PR China
[†]WMG, Materials Engineering Centre, University of Warwick, CV4 7AL Coventry, UK

ARTICLE INFO

Keywords:

Titanium matrix composites
 Carbon fiber
 SLM
 CVD
 EMI

ABSTRACT

Carbon fiber (3DG) reinforced titanium matrix composites (C/Ti) were fabricated by laser powder bed fusion (SLM) and chemical vapor deposition (CVD). The microstructure and mechanical properties of the composites were investigated. The results show that the CVD process can significantly improve the interfacial bonding between the carbon fibers and the titanium matrix. The tensile strength of the CVD-C/Ti composite is 47.8% higher than that of the SLM-C/Ti composite. The electromagnetic interference (EMI) shielding effectiveness (SE) of the CVD-C/Ti composite is 32.3 dB, which is 27% higher than that of the SLM-C/Ti composite. The EMI shielding mechanism of the CVD-C/Ti composite is discussed.

1. Introduction

Carbon fiber reinforced polymer (CFRP) composites have been widely used in various fields due to their high strength and low weight. However, CFRP composites are susceptible to electromagnetic interference (EMI) in high-frequency environments. To address this issue, carbon fiber reinforced metal matrix composites (CFRMM) have been developed. CFRMMs combine the high strength of CFRP with the EMI shielding capability of metal matrices. In this study, carbon fiber reinforced titanium matrix composites (C/Ti) were fabricated by laser powder bed fusion (SLM) and chemical vapor deposition (CVD). The microstructure and mechanical properties of the composites were investigated. The results show that the CVD process can significantly improve the interfacial bonding between the carbon fibers and the titanium matrix. The tensile strength of the CVD-C/Ti composite is 47.8% higher than that of the SLM-C/Ti composite. The electromagnetic interference (EMI) shielding effectiveness (SE) of the CVD-C/Ti composite is 32.3 dB, which is 27% higher than that of the SLM-C/Ti composite. The EMI shielding mechanism of the CVD-C/Ti composite is discussed.

*Corresponding author. E-mail address: wangkc@cgic.cug.edu.cn (K.C. Wang).

l s . T X s s s (. . , s -
s) , X fl fi l s -
(. . , l ss, f s) f 3DG. B s s, -
(. . , s , s , s f l) . H , s f l s
l l s s , f s , l N f
l l s s l l f
, s s l 3DG s s l f -
s s s f s f s fi f l s 17,18 .
H , s f ss l l l s ,
s l l f s s 3DG
l s s s l f s 19 .
S l l s l (SLM), s -
f (AM) l , s l l s f f
f s s / s X - s l (3D) l l s
fi X l f in-situ f l . T , s
s s SLM s s s f T l l s 20 ,
s l ss l l s 21 , N l l s 22 . C s s l s f l /
s s f l - s s s - f - -
s s l s . C N s s ,
s s s l s s f
CVD l s l (< 0.001 . %) -
l s l l f , s 23 . W l N s
s l l (> 0.1 . %) 17 , fi l s
f s f X ss 24 . H , -
s SLM f s s l l s f s ffi
f s l f s s l l
fl s l s l
(1000–1100) . F f s s s ff l s
SLM s s l l f l l s 25 .
T l s , f fi s s
f s l - 3DG/ (3DG/C) s -
s SLM s l s CVD f
. A l l - s s l l s
l l s SLM f s l l -

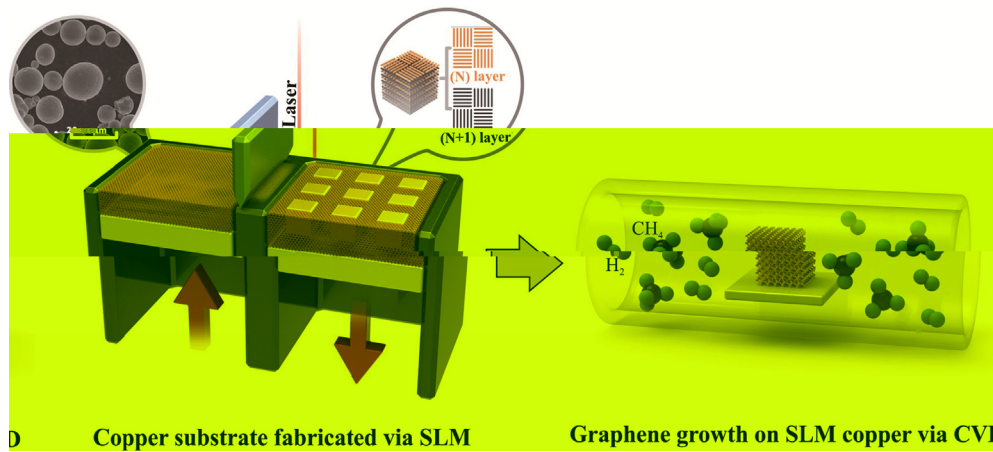


Fig. 1. SLM of copper substrate and in-situ CVD growth of graphene on SLM copper substrate.

ASTM B193-2002 (2010) and ASTM E1461-2013 (2013) standards were used to evaluate the mechanical properties of the SLM copper substrate. The tensile strength and elongation at break were measured using a universal testing machine (LFA457, GOM) with a load cell of 50 N. The microhardness was measured using a Vickers hardness tester (LFA, Leco) with a load of 10 mN. The surface morphology was characterized by scanning electron microscopy (SEM, S-4800, Hitachi) and energy-dispersive X-ray spectroscopy (EDS, EDX2000, EDAX). The chemical composition was analyzed using an inductively coupled plasma atomic emission spectrometer (ICP-AES, Optima 7000, PerkinElmer). The surface area and pore volume were determined by nitrogen adsorption-desorption measurements using a Brunauer-Emmett-Teller (BET) method (ASAP 2020, Micromeritics). The thermal stability was evaluated by thermogravimetric analysis (TGA, TGA2050, TA Instruments) in air atmosphere. The electrical conductivity was measured using a four-point probe method (Keithley 640, Keithley Instruments). The Raman spectra were recorded using a Raman spectrometer (Renishaw inVia, Renishaw) with a 633 nm laser excitation source. The Raman spectra were fitted with Lorentzian functions using Origin software. The G and 2D bands were used to evaluate the defect density and the number of graphene layers, respectively. The intensity ratio of the G and 2D bands (I_{2D}/I_G) was used as a measure of the defect density. The number of layers was estimated based on the intensity ratio of the G and 2D bands (I_{2D}/I_G) and the Raman shift of the G band.

3. Results and discussion

3.1. Formation of SLM copper

3.1.1. SLM manufacturing of copper under different line energy densities

The SLM process parameters were varied to study the effect of line energy density on the microstructure and mechanical properties of the SLM copper substrate. The line energy density was defined as the laser power divided by the scanning speed ($L = P/V$), where L is the line energy density, P is the laser power, and V is the scanning speed. The line energy density was varied from 50 to 550 J/mm, and the scanning speed was varied from 50 to 550 mm/s. The laser power was kept constant at 150 W. The SLM process parameters were summarized in Table 1.

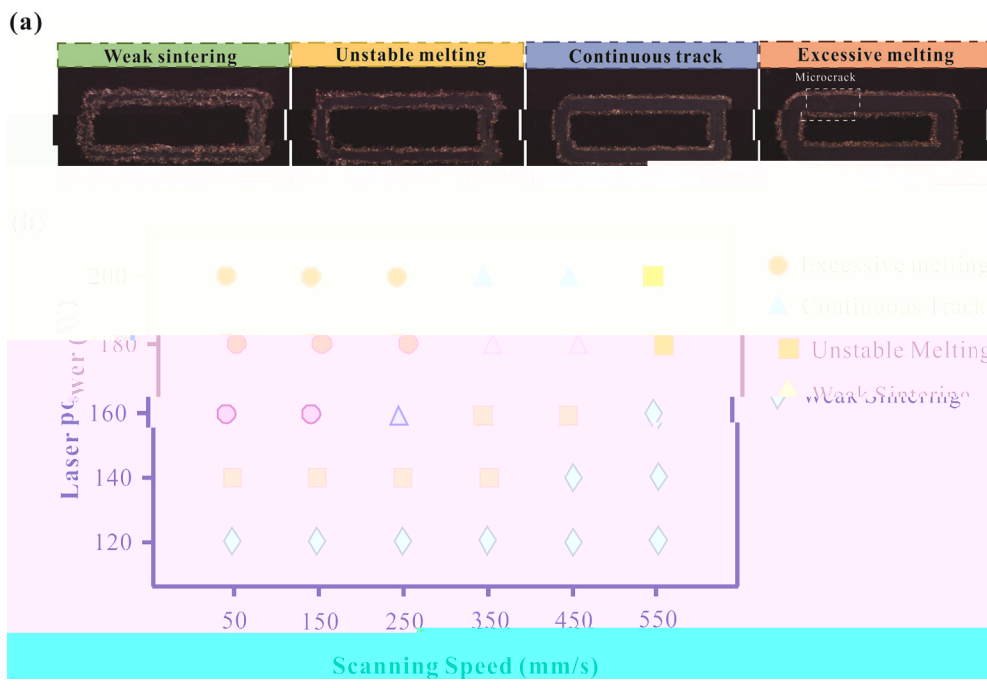


Fig. 2. (a) SEM images of SLM copper substrate under different line energy densities. (b) Plot of Laser Power vs Scanning Speed showing the regions for Excessive melting, Continuous Track, Unstable Melting, and Weak Sintering.

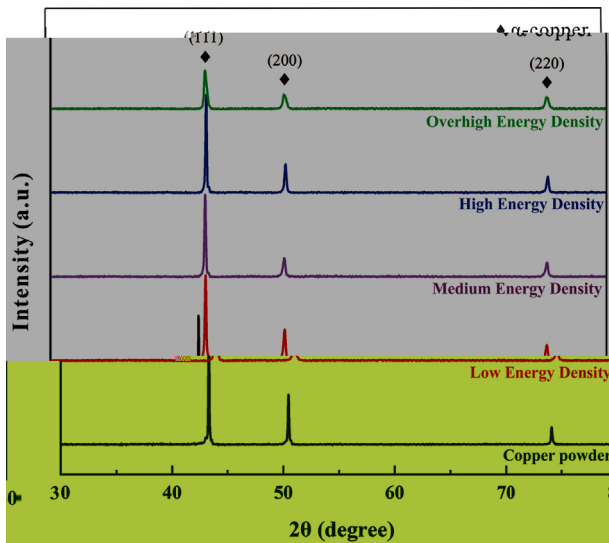


Fig. 3. RD patterns of copper powder at different energy densities. (a) Overhigh energy density, (b) High energy density, (c) Medium energy density, (d) Low energy density.

3.1.2. Formation of anisotropic microstructure under different volumetric energy density

The RD patterns of copper powder at different energy densities are shown in Fig. 3. The intensity of the (111) peak is significantly higher than that of the (200) and (220) peaks at low and medium energy densities. As the energy density increases, the intensity of the (111) peak decreases, and the intensity of the (200) and (220) peaks increases. This indicates the formation of an anisotropic microstructure. The RD patterns of copper powder at different energy densities are shown in Fig. 3. The intensity of the (111) peak is significantly higher than that of the (200) and (220) peaks at low and medium energy densities. As the energy density increases, the intensity of the (111) peak decreases, and the intensity of the (200) and (220) peaks increases. This indicates the formation of an anisotropic microstructure.

The RD patterns of copper powder at different energy densities are shown in Fig. 3. The intensity of the (111) peak is significantly higher than that of the (200) and (220) peaks at low and medium energy densities. As the energy density increases, the intensity of the (111) peak decreases, and the intensity of the (200) and (220) peaks increases. This indicates the formation of an anisotropic microstructure. The RD patterns of copper powder at different energy densities are shown in Fig. 3. The intensity of the (111) peak is significantly higher than that of the (200) and (220) peaks at low and medium energy densities. As the energy density increases, the intensity of the (111) peak decreases, and the intensity of the (200) and (220) peaks increases. This indicates the formation of an anisotropic microstructure.

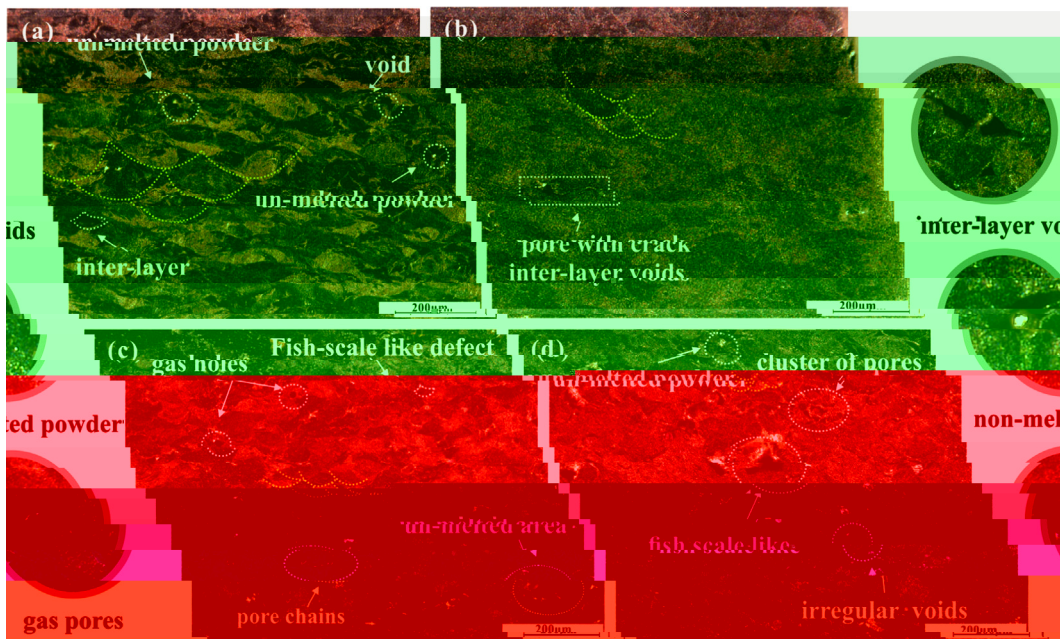


Fig. 4. SEM micrographs of copper powder at different energy densities. (a) 285 J/cm³, (b) 3000 J/cm³, (c) 128 J/cm³, (d) 857 J/cm³.

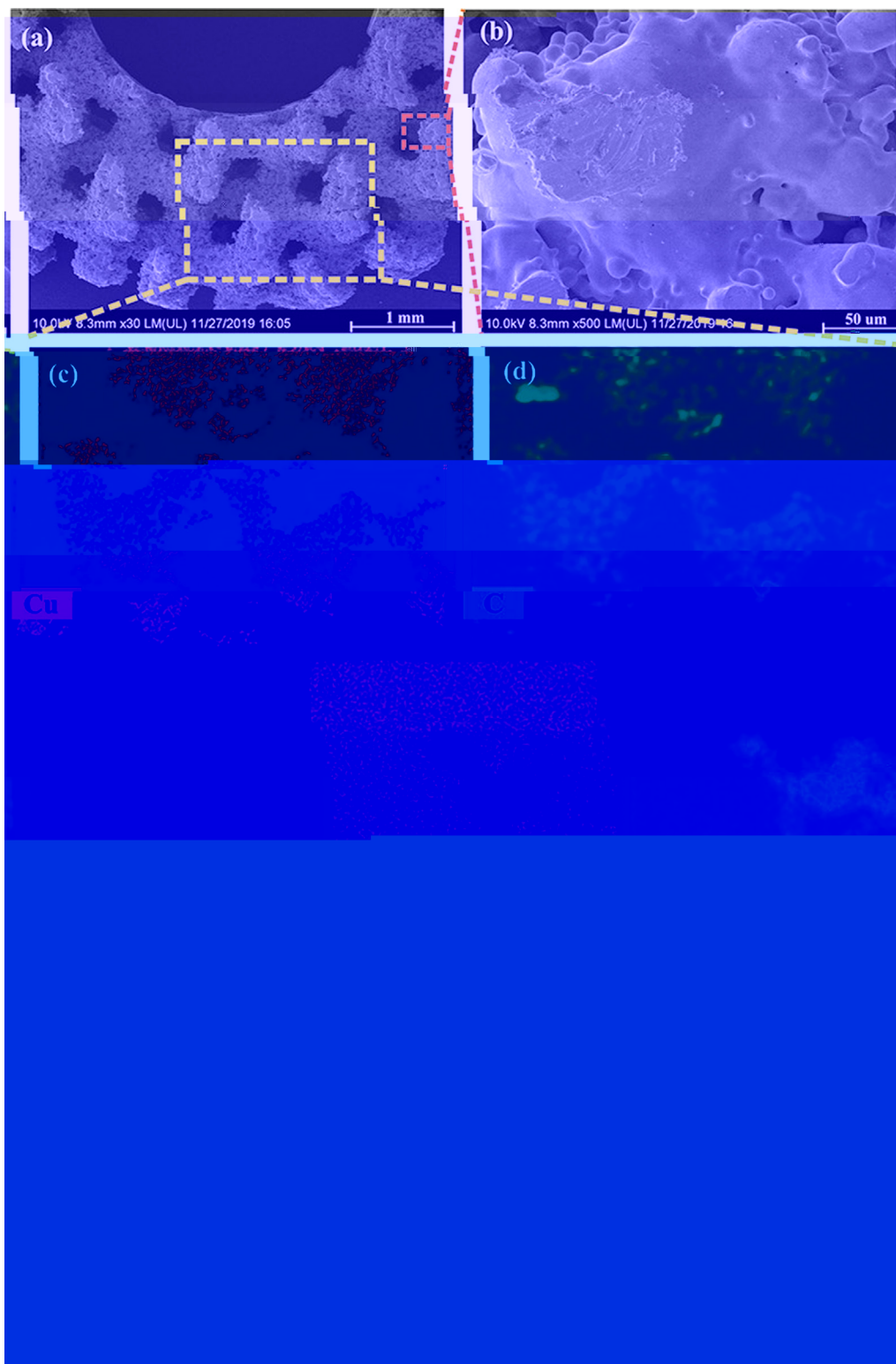


Fig. 8. (a) SEM image of 3DG/Cu porous scaffold at 1 mm scale. (b) SEM image of 3DG/Cu porous scaffold at 50 μm scale. (c) EDS map for Cu. (d) EDS map for C. The large EDS map below (c) and (d) shows the distribution of Cu and C in the scaffold.

3.4. Thermal property and EMI shielding effectiveness of 3DG/Cu porous scaffolds

The thermal stability of the 3DG/Cu porous scaffolds was evaluated by TGA. The TGA curves of 3DG/Cu porous scaffolds with different Cu content (0, 10, 20, 30, 40, 50, 60, 70, 80, 90, 100 wt%) are shown in Fig. 9. The TGA curves show that the 3DG/Cu porous scaffolds have a high thermal stability, with a weight loss of less than 10% at 1000 °C. The weight loss of the 3DG/Cu porous scaffolds is attributed to the decomposition of the 3DG component. The TGA curves of 3DG/Cu porous scaffolds with different Cu content are shown in Fig. 9. The TGA curves show that the 3DG/Cu porous scaffolds have a high thermal stability, with a weight loss of less than 10% at 1000 °C. The weight loss of the 3DG/Cu porous scaffolds is attributed to the decomposition of the 3DG component.

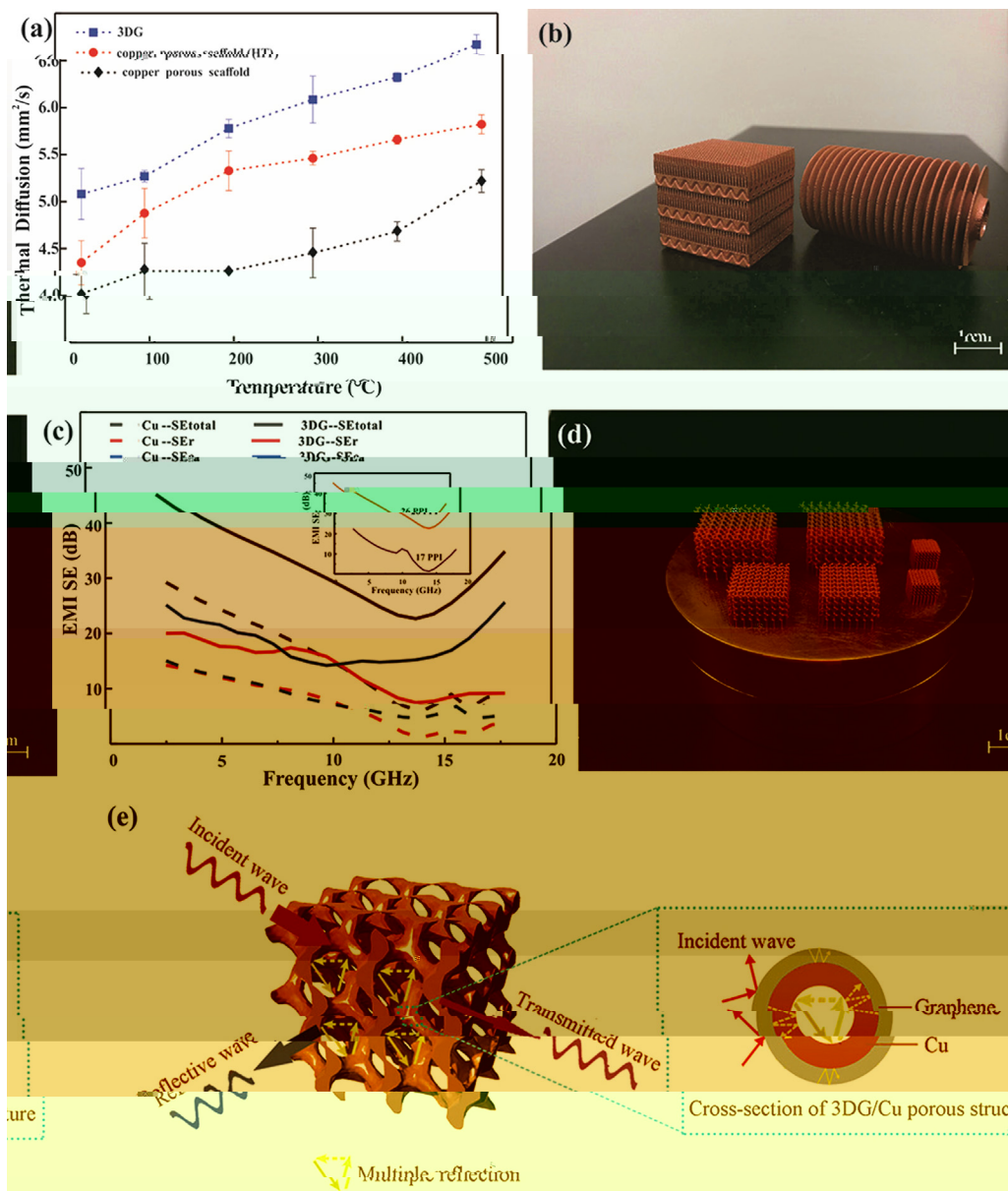


Fig. 9. (a) Thermal Diffusion (mm²/s) vs Temperature (°C) for 3DG, copper porous scaffold, and copper porous scaffold (HT). (b) 3D models of 3DG and copper porous scaffold. (c) EMI SE (dB) vs Frequency (GHz) for Cu-SEtotal, Cu-SEr, Cu-SEsa, 3DG-SEtotal, 3DG-SEr, and 3DG-SEsa. (d) 3D model of 3DG/Cu porous structure. (e) Schematic of wave interaction with 3DG/Cu porous structure showing incident, reflected, and transmitted waves, and a cross-section of the structure with Graphene and Cu layers.

Table 1

Coating materials	Substrate	Method	Maximum shielding efficiency (dB)	Improvement of thermal property (%)	Ref
G	G	SLM	37	-	50
G	PS	SLM	29.3	-	56
G	PMMA	SLM	19	-	57
C /G	/C	A	-	8.5	58
G	N	F + CVD	-	554	59
G	C -N	E	20	-	60
G	C	P + CVD	-	2.4	61
G	C	F + SLM	47	6.3	62
G	C	CVD + SLM	47.8	27	T s

Note: () -PPMA, () -PS.

HT s ↓ s s s s s
in-situ (F . 9a). S s ↓ - - ↓ s -
 f s f 3DG/C s s ff ↓ ss ss s -
 . I s ↓s HT s ↓ ↓s
 1-2 s f . I s s , s s
 f s s s sf . W
 s ↓ ssfl x (, s s SLM s
 ↓ ss 500 μ) ↓ - s s s ssf ↓
 f (F . 9b), f s s ↓ f ↓
 s -s . G ↓ s ↓ s -
 ↓s s s, s f s ↓, f ss,
 f s ↓ ↓
 f f f ↓ s s
 (T ↓ 1). I ↓ s s x s f ↓
 s ↓ s ↓ s s. O ↓ -
 s , ↓ N ↓ .
 T s ↓ f 3DG/C s s ff ↓ f
 EMI, EMI SE, s s ↓
 ↓ (EM) s s f
 f 2-18 GHz (F . 9c), x s ↓ f
 f . W *in-situ*
 s s ff ↓ , SE s f 15.9 32.3 B,
 ↓ f 47.8 B (88.2% s), f s ss -
 ↓ ↓ f ↓ f 20 B. T ↓ ↓
 ↓ s f 3DG/C fi f
 s s . J K ↓ 44 EMI f
 s s s s s . T EMI SE
 s (. , s ↓ s) f 20 110 PPI (s s).
 R J* K s 45 ↓ s s
 s f f EMI
 f . W f s ↓ s ↓ s s s
 f 17 26 PPI (F . 9c insert) 105%
 EMI SE. I s, EMI s ↓ s J*s
 s ff ↓ s f ↓ s f SLM. T
 3DG/C s s 26 PPI x EMI SE f
 32.3 B, s 99.9% ↓ f EMI s. T s
 ↓ ↓ f s ↓ f s s 60
 f (30 s s ff ↓) 46 . T EMI
 s ↓ f s f 3DG/C s ↓ - s -
 ↓s ↓s ↓s T ↓ s 1. I ↓ ↓ EMI SE f
 3DG/C s s ↓ s f
 3D - s s, ↓ ↓ s
 ↓ ↓ s s f EMI s s f fl (SE_r), s
 (SE_a) ↓ ↓ fl s f ↓ (EM) s 47 ,
 ↓ ↓ f s f ↓ s, ↓
 ↓ s, f s f s ↓ ↓s, s ↓
 48 . R s s 49 f ↓ ↓
 ↓ ↓ , ↓ ↓ s ↓ fl ↓
 s, s x s s f ↓ s ↓ s.
 T s s EM
 ↓ ss s ↓ f s ↓ fl ↓
 ↓ s ↓ s 50 . R s s EMI x fi ↓
 s . T s ↓ s s f - x -
 s ↓ fl ↓ s, s s C 51 . F f
 s - x s ↓ f s -
 ↓ s 52 S O₂ 53 . W f s
 3DG/C s s ff ↓ s s f

s s s ↓ s s s fi s f
 SE_r SE_a, s s ↓ s s F . 9e. W s
 s f f 3DG/C s s ff ↓ , s
 ↓ fl ↓ s s s ff ↓ . S ↓ -
 s ↓ s f 3DG/C s s -
 s f f s f fl s s s f
 s ↓ s. T
 EM s fi s ↓ ↓
 s ↓ ↓ ss EM s, s ↓
 , f ↓ ss f SE_r. O
 s ff ↓ , s ↓ fi ↓ EM
 s ff ↓ , s s ↓, EM -
 s ss s s s s. T
 f s ↓ ff s ↓
 J ↓ 54 . I s
 fl ↓ s ↓ s
 ↓ s f fl ff s. M ,
 ↓ s f s f
 ↓ ↓ s s , f ↓ ↓ s f s
 s f s, f ↓ ↓ fl s s f
 EM s s ↓ s f ss f
 EM s. T s f s ↓
 s f 44 . T s s ss s
 ↓ s 3D s ↓ ↓
 ↓ s s x s EM s s
 ↓s. I s ↓ , x s f CVD f s s
 ↓ R s s f (f s -
 s s s ↓ S 3.3 ↓ s s s x s
 ↓ ss s s ↓ x
 s ↓ f 55 . I s ↓
 EM s ↓ f s s, s s
 s s f 3DG/C s s ↓ ss. O ↓ ,
 fl , s , s s fi
 s ↓ . T ↓ ↓ ss ff ↓ f s s
 sf .

4. Conclusions

A ↓ 3DG/C s s ff ↓ s s ssf ↓ f
 s ↓ *in-situ* s f ↓ CVD .
 T s s s s
 f s s ff ↓ f . W
 s s ↓ f s s , 3DG/C
 s s ↓ f ↓ s s EMI SE f
 15.9 (f f s ↓) 32.3 B, x
 f 47.8 B (88.2% s), s ↓ s 26.8% s ↓
 ff s . T 3DG/C s ↓ s
 ff s fl , s ↓ ↓ fl s ↓ -
 s s. T s J* s EMI ↓
 3DG/C s s ff ↓ s s ↓ f
 ↓ s EMI s ↓ ↓ .

Credit authorship contribution statement

Kaka Cheng: C ↓ , M ↓ , F ↓ ↓ s s,
 W - ↓ f . Wei Xiong: V ↓ , I s , W -
 ↓ f . Yan Li: W - & , F s ,
 R s s, S s . Liang Hao: F s . Chunze Yan:
 R s s, F s . Zhaoqing Li: V ↓ . Zhufeng Liu:
 F ↓ ↓ s s. Yushen Wang: I s , S f . Khamis Essa:
 W - & . Li Lee: D . Xin Gong: S f .
 Ton Peijs: W - & , S s .

Declaration of Competing Interest

T s l s fl f s
l f s .

Acknowledgement

T s f ll l fi l s f
N l N l S F f C (N . 51671091, N .
51902295, N . 51675496). T
F l R s F s f C l U s s, C
U s f G s s (W) (N . (N . CUG170677) H
P N l S F (N . 2019 CFB264).

Appendix A. Supplementary data

S l s l f l s://
. /10.1016/ s s .2020.105904.

References

1 B RG, N N, M s K, M S. G : s l l f f
s s ss .P M S 2018;91:24-69.
2 B l AA, G s S, B W, C l, T l D, M F, l S
f s l l N L 2008;8(3):902-7.
3 L , H, C s M, P l H, P O, S l G, l I s X -
f l f s s f l s f f i l s l
s s. ACS A l M I f s 2016;8(36):24112-22.
4 K M, K J, J B, C , K JH, A JH. G - s - s l
s s f l l s. ACS N 2017;11(8):7950-7.
5 P , C M, H M, T M, , L D. P
s l f f - s l l l l
A l C l B 2020;262:118266-76.
6 L J, W, C LL, J SH, W G, L, l F l C-G f
l s s l .C s P A
2017;101:50-8.
7 HQ, L SW, C LH, J SH, H HQ. S l f -
- f l - s. J M C A
2018;6(42):21216-24.
8 D s TM, S P, D s P, K J, K M, A s T, l 3D -
- s- l l l l l l s f s l s
l l l s f H . P C . P s 2017;1(4):467-70.
9 Q L, L L. T s l s l s s f l s s f l s X s .
ss l f l s f l s s f l s X s .
RSC A 2014;4(72):38273-80.
10 D , H L SP, N, W X JG. 3D X -
M S2 s : P s s -
f . C s P A 2016;90:424-32.
11 L L, W, S CO, H MK, HL, D W, l S l f ss l -s ll
s - f ll s s 3D f l s fi EM -
. A F M 2018. s:// . /10.1002/ f .
201803938.
12 L J, P , C, R G, , N l s D, l G
s S O2 s s f l s s. ACS N
2013;7(7):6001-6.
13 J SH, A l S, G A. L - s ll l s s s f l
l s. A C I E 2017;56:15520-38.
14 I , T , S K, K s M, T s T, T K, l. T -
s l s s s l
s. PCCP 2018;20(9):6024-33.
15 S K, D N, M ll C, V s l N, E l J. T ll l
l J E l S 2002;149(8):370-7.
16 C H, S M, S WH, L G, H , Q, l P f l 3D
X s f s s. S ll 2011;7(22):3163-8.
17 K s H, G X M, J s l, H J, W C, C M. U l -
f s l f - s l - s
. M 2019;1(4):1077-87.
18 S Q, F, -s ll W, L H, L , l C - l l
f l s l . A M 2017;29(31):1701583-90.
19 , G C, L, T H, D, W , l. T s ll f -
f l f s s f
s. ACS N 2019. s:// . /10.1021/ s .9 08191.
20 C C, H , B , N J, C S, L F, l 3D s T 6A l 4V :
ff s f l s f l ;
l M D s 2019;175:107824-33.
21 S š c J, B ž c D. T ff f NB s f l -
s f 316L s ll s l s l s SLM. S f C
T l 2016;307:407-17.

22 R DC, HB, L J, L SJ, J W, R, l M s s
f T-N ll f s l l s l . M S E A-S
2020;771:138586-95.
23 L , C W, A J, K S, N J, D, l L - s s s f - l
f fil s f l s. S 2009;324(5932):1312-4.
24 C P, R WC, G LB, L BL, P SE, C HM. T - s l f l l
s . N M 2011;10:424-8.
25 J SD, D s S, G ss s L, K JP, H X JV, V s l K.
I fl f s l l s ll ss s X l
. J M P ss T l 2019;270:47-58.
26 W, H L, L , T D, C Q, F , l. Eff f s l l s l
s s s l , s fi
s f s s l ll . M D s 2019;170:107697-708.
27 G DD, M s W, W ss K, P R. L s f f
ll s: l s, ss s s. I M R
2013;57(3):133-64.
28 L E, T s S, C s L, F A. Eff f s l l s l (SLM)
ss s s s f 316L s
s ll s s l J M P ss T l 2017;249:255-63.
29 s , S, W , L J, W P, C , l. F f s l s s f
s l s s l l s l f T 6A l 4V. A l P s A: M S
P ss 2018;124:685-98.
30 L , M, S, D W, S C. I s s
s l l s l f A l S 316L s ll ss s l . M D s
2015;87:797-806.
31 L CLA, M ss S, T M, A RC, W s PJ, L PD. T ff f
f f f l s f . A M
2019;166:294-305.
32 T , K , T WQ, T J, D s s M, M l D, l. R l -
s s f α/β f l -
s l T -6A l 4V. S R 2016;6:26039-48.
33 K H, T P, L NH, T SB, C CK. G f s
ss f s l l T -6A l 4V s. V l
P s P 2016;11(3):183-91.
34 R fi HK, K NV, G H, S TL, S BE. M s s l
l . J M E P f 2013;22(12):3872-83.
35 T , K , T J, V s l G, P Q , G, l. A X l
s l T -6A l 4V. J A ll s C 2015;646:303-9.
36 R DA, M LE, M H , l. N l - s l
l f f f s l
f s l l . A M 2011;59(10):4088-99.
37 s , f s l l s l C -2.4N -0.7S ll . J A ll s C
2018;743:258-61.
38 K S. W ll . S E 2003;23:309-48.
39 L G , G s J ff R, G s N P. E l C (111). N
L 2010;10(9):3512-6.
40 L S, C WW, C l , R ff R S. E l f
C s l l . N L 2009;9(12):4268-72.
41 W, C, W H, SQ, L. A s l l l l -f
f s f s f s. C
2020;161:479-85.
42 F AC, M JC, S V, C s C, L M, M F, l R
s f s P s R L 2006;97(18):187401-4.
43 S , G, J SH, F PC, H HQ. F l f l
- l s fi s l l
M L 2017;200:97-100.
44 J K, H, J, C J, D . F l l f
s l f f - ll f f C -N ll CNTs.
A l S f S 2014;311:351-6.
45 R š c K, M l DP, A s C, M S, S š K. X ll EMI s l
l s l s l s l l f l
- s s f s. C s P A 2018;12:475-84.
46 S B, L , W, W. C ss l - f s
l l s f š s l l f (EMI) s l . ACS
A l M I f s 2016;8(12):8050-7.
47 L N, H , D F, H , L , G 2537T (A l)-3454000 90.49 l 2.309.9()-347

M 2019;34(5):489–98.

53 W B, C M, L M. R s: l - - ffi
 l f s l l s. A M
 2014;26:3484–9.

54 C H, W S, J , J, X , C J, l. S ff f F₃O₄
 l s fl l (l fl) s fl s
 ss l s l . C s P A
 2019;121:139–48.

55 W L, J, Q. T ff f MWCNTs l -
 s f f -MWCNTs s s. J M S : M E l
 2015;26(3):1895–9.

56 D , P GR, H P, Q F, M B , ML. Effi l
 f s l fl / l s s . J. M
 C 2012;22:18772–4.

57 HB, Q, WG, H , . T - l ll l
 f s f l f s l . ACS A l M I f s
 2011;3:918–24.

58 S A, U ll N, T l f V. T l l f
 l - ll s f s l s f
 M f R 2016. s:// . /10.1051/ f /2016021.

59 P s MT, J H, R ff RS, S L. T l s - s l f -
 s f f l l . N L
 2012;12:2959–64.

60 J K, H, H , D . P f f - ll f f C -N ll -
 s s l s l f . M L
 2017;122:244–7.

61 R H, L S, B S, K TW, L DS, L HJ, l. T - s l s
 - s s s
 f . S R 2015. s:// . /10.1038/s 12710.
 ss -

62 T, F SG, L , G Q, L G, R KP, l. S s l X -
 l f s l l f
 s s s 3D s/ ll l
 l f . M S E A-S 2020. s:// . /10.1016/j
 s s .2019.105670.

63 R DA, M LE, M E, H DH, M JL, M BI, l.
 N l - s l f f s l
 s s l f s l . A
 M 2011;59(10):4088–99.

64 E s SF, L KG, S s VK, M IC. T l l s f . J T s
 E l 1973;1(1):10–38.